Journal of Lake Sciences, Vol. 10, Suppl., pp447-475, 1998.

The Role of Advection and Stratification in Wind-driven Diffusion Problems of Alpine Lakes*

Kolumban Hutter and Yongqi Wang
Institute of Mechanics, Darmstadt University of Technology
Hochschulstr. 1, D-64289 Darmstadt, Germany

Abstract: *A semi-implicit semi-spectral hydrodynamic primitive equation model is used to study tracer diffusion in homogeneous and stratified lakes. Impulsively applied spatially uniform wind is applied in the long direction of a rectangular basin with constant depth and Lake Constance. Tracer mass is released at various locations of the free surface and its spreading under the action of diffusion and advection is studied.We show that for homogeneous basins the tracer quickly spreads over the entire water depth. Inertial waves can also be detected in the tracer concentration. On the other hand for stratified waters the tracer mass is largely confined to the epilimnion with occasional penetration into the hypolimnion where large downwelling occurs. Here Kelvin- and Poincar 'e-type wave dynamics is discernable in the tracer-concentration-time series, the former more conspicuously at nearshore, the latter at off-shore positions.*
Keywords: *Tracer diffusion, lake circulation, limnology, oscillation.*

1. Introduction

Lakes are physical systems that respond to the input of solar radiation and wind. Their current distributions to a given wind scenario depend on the stratification, i. e., mass distribution that prevails prior to a certain wind scenario, and this stratification is established by the long term seasonal variation of this thermal input. If a tracer - natural or artificial - is entering a lake through its rivers or via the free surface, this tracer is dispersed and distributed in the lake according to as much it is subject to (turbulent) diffusion and advection. Both are to a certain extent determined by the circulation flow established by the wind. It follows that the dispersion of a tracer in a lake is largely determined by the flow that is established and that the particular features in the flow should also be recognizable in the evolution of the tracer concentration.

We complement a pure hydrodynamic semi-implicit semi-spectral model SPEM (Haidvogel *et al* 1991, Wang & Hutter 1998) by a semi-implicit spectral model for diffusion and demonstrate its suitability in various scenarios of tracer diffusion for homogeneous and stratified lakes. We consider a rectangular basin of constant depth and dimension 65×17 km^2×100 m and study tracer dif-

* Received 1997-02-25; accepted 1998-03-27

fusion when the tracer mass is released at various locations of the free surface. The basin is subjected to an external wind, impulsively and spatially uniformly applied in the long direction of the rectangle. We repeat similar scenarios for Lake Constance (bordering Austria, Germany and Switzerland) and show that, qualitatively, very similar behaviour can be observed.

We demonstrate that in homogeneous water a tracer substance is relatively rapidly distributed over the entire depth of the basin, that the absolute values of the diffusion at a given location depend rather crucially on the direction of the flow at a given location. Inertial wave dynamics has an influence on the early time behaviour of the tracer distribution. This behaviour is seen with both, the rectangular basin and Lake Constance.

For a stratified lake with a tracer mass that is released on the free surface this tracer mass is practically distributed only in the upper layer with some, though limited, penetration into the hypolimnion where downwelling is particularly significant. The wave dynamics that can be seen are now Kelvin waves and Poincaré waves, and both are seen at early times of a surfacial tracer dispersion. Kelvin waves are particularly pronounced at near shore positions, while Poincaré waves show at off-shore positions, but traces of both have been seen at all locations where tracer has been released.

In section 2 we list the governing equations, section 3 deals with the numerical peculiarities, section 4 lists the parameters of the turbulent closure conditions and the temperature distribution. Sections 5 and 6 deal with the tracer diffusion in a rectangle of constant depth and in Lake Constance, respectively. Both homogeneous and stratified conditions are studied. Finally, in section 7 we summarize the results and point at further possible work.

2. Governing equations

These comprise of the field equations valid in the domain occupied by the water and the boundary conditions along the free surface and the lake bottom that bound the lake domain.

2.1 Balance laws of mass, momentum and energy

We assume that the water is "contaminated" by a tracer or a number of tracers, but that their concentration is so minute that the density of the mixture, i. e., water plus tracers is not affected by the presence of the latter. Thus, the balance laws of mass for the mixture and each tracer and the balances of linear momentum and energy for the mixture together with the thermal equation of state form the field equations for the considered fluid system. We impose the Boussinesq assumption (which states that density variations only affect the buoyancy force) and also employ the shallow water assumption (which asserts that physical variables change much slower over horizontal distances than over vertical ones). Thus, the field equations read

$$\frac{\partial u}{\partial x} + \frac{\partial v}{\partial y} + \frac{\partial w}{\partial z} = 0 \tag{1}$$

$$\frac{\partial c_\alpha}{\partial t} + \vec{v} \cdot \nabla c_\alpha = \frac{\partial}{\partial x}\left(D_H^{c_\alpha} \frac{\partial c_\alpha}{\partial x} \right) + \frac{\partial}{\partial y}\left(D_H^{c_\alpha} \frac{\partial c_\alpha}{\partial y} \right) + \frac{\partial}{\partial z}\left(D_v^{c_\alpha} \frac{\partial c_\alpha}{\partial z} \right), \quad (\alpha = 1,\ldots, \upsilon) \tag{2}$$

$$\frac{\partial u}{\partial t} + \vec{v} \cdot \nabla u - fv = -\frac{\partial \phi}{\partial y} + \frac{\partial}{\partial x}\left(\nu_H \frac{\partial u}{\partial x}\right) + \frac{\partial}{\partial y}\left(\nu_H \frac{\partial u}{\partial y}\right) + \frac{\partial}{\partial z}\left(\nu_v \frac{\partial u}{\partial z}\right), \tag{3}$$

$$\frac{\partial v}{\partial t} + \vec{v} \cdot \nabla v + fu = -\frac{\partial \phi}{\partial y} + \frac{\partial}{\partial x}\left(\nu_H \frac{\partial v}{\partial x}\right) + \frac{\partial}{\partial y}\left(\nu_H \frac{\partial v}{\partial y}\right) + \frac{\partial}{\partial z}\left(\nu_v \frac{\partial v}{\partial z}\right), \tag{4}$$

$$0 = -\frac{\partial \phi}{\partial z} - \frac{\rho g}{\rho_0}, \tag{5}$$

$$\rho = \rho(T), \tag{6}$$

$$\frac{\partial T}{\partial t} + \vec{v} \cdot \nabla T = \frac{\partial}{\partial x}\left(D_H^T \frac{\partial T}{\partial x}\right) + \frac{\partial}{\partial y}\left(D_H^T \frac{\partial T}{\partial y}\right) + \frac{\partial}{\partial z}\left(D_V^T \frac{\partial T}{\partial z}\right). \tag{7}$$

Here a Cartesian coordinate system (x,y,z) has been used; (x,y) are horizontal, and z is vertically upwards, against the direction of gravity. The field variables and parameters arising in (1) - (7) are defined in Table 1. Eq.(1) expresses conservation of mass for the mixture in the Boussinesq approximation; (2) is the mass balance for constituent α^1; here diffusion is accounted for by postulating Fick's first law for the constituent mass flux in the form

$$\vec{j}^{\alpha} = -\rho\left(D_H^{c_\alpha} \frac{\partial c_\alpha}{\partial x}, D_H^{c_\alpha} \frac{\partial c_\alpha}{\partial y}, D_V^{c_\alpha} \frac{\partial c_\alpha}{\partial z}\right), \tag{8}$$

which introduces orthotropic diffusive behaviour, equal in both horizontal directions but different in the vertical direction. Eqs. (3) and (4) are the horizontal components of the momentum equation, also accounting for momentum diffusion different in the vertical and the two horizontal directions and expressed by the turbulent viscosities υ_V and υ_H, respectively. Eq. (5) is the hydrostatic pressure equation, a consequence of the shallow water assumption. Eq. (6) is the thermal equation of state, here used in the form

$$\frac{\rho - \rho_0}{\rho} = -\beta(T - T_0)^2, \tag{9}$$

valid to a sufficient degree of accuracy for T∈ [0, 40]°C. The fact that dependencies on impurities (salt) and pressure are ignored restricts considerations to fresh water lakes with moderate depths. Eq. (7) is the balance of internal energy; it accounts through Fourier's heat law

$$\vec{q} = -\rho c_v \left(D_H^T \frac{\partial T}{\partial x}, D_H^T \frac{\partial T}{\partial y}, D_V^T \frac{\partial T}{\partial z}\right) \tag{10}$$

for orthotropic thermal turbulent diffusion, but not for radiation; so no seasonal variations of the thermocline are in focus. Nevertheless, changes of the temperature distribution, and therefore density distribution, can be accounted for, but not if they are due to solar irridation. In principle, incorporation of radiation is, however, straightforward.

2.2 Boundary conditions for mass, momentum and energy

The above laws comprise 5 +v field equations for the fields $\vec{v}$, c^α, ϕ and T which are also 5 +v unknown fields. As partial differential equations of second order in the space variables they must be subjected to boundary conditions of both kinematic and dynamic nature. Let the undeformed free surface be described by $z = 0$ and let the base be described by $z = h(x,y)$. We shall

formulate the boundary conditions on these surfaces. This implies that the *rigid lid assumption* will be imposed; it eliminates all barotropic surface gravity waves but still incorporates topographically induced barotropic oscillations.

2.2.1 Mechanical and thermal conditions

With the above restrictions the kinematic conditions read

$$\left.\begin{aligned} -w &= 0, && at \quad z = 0 \\ -\vec{v}\cdot\nabla h - w &= 0, && at \quad z = -h(x,y) \end{aligned}\right\} \tag{11}$$

here $\vec{v}_H = (u, v)$, and ∇ is the (horizontal) gradient operator.

As for the dynamic boundary conditions it is customary to relate the shear tractions at the free surface to the horizontal components of the wind velocity at the 10 m level. An analogous parameterization is used at the bottom: the shear tractions are related to the basal velocity components. As for the thermal boundary conditions, if time spans over which the equations are integrated are not too large, one generally ignores an exchange of sensible heat between the water and the atmosphere and bottom, respectively. Thus, the dynamic boundary conditions take the forms at the free surface $z = 0$:

$$\left.\begin{aligned} (\tau_x^0, \tau_y^0) &= \rho_a c_0 \sqrt{U^2 + V^2}\,(U, V), \\ \frac{\partial T}{\partial z} &= 0, \end{aligned}\right\} \tag{12}$$

at the bottom surface $z = -h(x, y)$:

$$\left.\begin{aligned} (\tau_x^h, \tau_y^h) &= \rho_a \gamma_h (u_h, v_h), \\ Q_{geoth} - \frac{\partial T}{\partial z} &= 0, \end{aligned}\right\} \tag{13}$$

In these equations, $\tau_{x,y}^0$ are the horizontal components of the shear tractions exerted by the wind on the water surface, ρ_a is the density of air, c_0 is the drag coefficient, and (U, V) are the horizontal velocity components of the wind 10 m above the free surface. Similarly, $\tau_{x,y}^h$ are the shear tractions exerted by the bottom on the water, γ_h ($\approx 10^{-3} \div 10^{-4}$ m·s^{-1}) is the frictional coefficient and (u_h, v_h) are the horizontal water current components at the bottom. Q_{geoth} is the geothermal temperature gradient. All these quantities are also listed in Table 1.

2.2.2 Boundary conditions for the tracer mass flux

It shall be assumed that any tracer mass can only be brought into the water body via the river inflows and by a source at the free surface of the lake. By the same token it can leave the lake domain only through its exit rivers and by sedimentation at the bottom surface. Thus one prescribes an inflow

$$\vec{j}^{\alpha}\cdot\vec{n} = j_w^{\alpha}, \quad \text{at inflow coordinates when} \quad \vec{v}\cdot\vec{n} < 0\,; \tag{14}$$

Tab. 1 Variables and parameters arising in the field equations and boundary conditions

c_a [mg·m^{-3}]	Mass density of constituent α (concentration)
c_v [Joule·kg^{-1}°C^{-1}]	Specific heat of water at constant volume
$c_0 \approx 0.0018$[-]if $\|U\| < 10$ m·s^{-1}	Drag coefficient for evaluation of wind stress
c_α^w [mg·m^{-3}]	Concentration of constituent α at the boundary when $\vec{v}\cdot\vec{n} > 0$
$D_H^{c\alpha}$, $D_V^{c\alpha}$ [m^2·s^{-1}]	Turbulent horizontal and vertical mass diffusivities of constituent α
D_H^T , D_V^T [m^2·s^{-1}]	Turbulent horizontal and vertical thermal diffusivities
$f = 2\Omega\sin\Phi$ [s^{-1}]	Coriolis parameter, where Ω is the anular velocity of the Earth and Φ the geographical latitude
$g=9.81$[m·s^{-2}]	Gravity constant
j_w^α [m^{-2}]	Concentration flow of constituent α at the boundary when $\vec{v}\cdot\vec{n} < 0$
Q_{geoth}[°C·m^{-1}]	Geothermal temperature gradient
T[°C]	Temperature
U, V[m·s^{-1}]	Horizontal components of the wind 10 m above water surface
u, v, w[m·s^{-1}]	Components of the water current in the x-, y-, z-directions
u_h, v_h[m·s^{-1}]	the horizontal water current components at the bottom
$\beta \approx 6.8\times10^{-6}$ [°C^{-2}]	Quadratic coefficient of thermal expansion
$\gamma_h \approx 10^{-3}\sim10^{-4}$[m·s^{-1}]	Bottom drag coefficient
$\phi = p/\rho$ [kgm^{-1}s^{-2}]	Dynamic normalized pressure
υ_H , υ_V [m^2·s^{-1}]	Kinematic turbulent horizontal and vertical momentum diffusivities (viscosities)
ρ[kg·m^{-3}]	Density of water
ρ_0[kg·m^{-3}]	Density of water at 4 °C
$\rho_a=1.225$[kg·m^{-3}]	Density of air

whilst outflow conditions are given by

$$\vec{j}^\alpha \cdot \vec{n} = c_w^\alpha \cdot \vec{v} \cdot \vec{n}, \quad \text{at outflow coordinates when} \quad \vec{v}\cdot\vec{n} > 0; \tag{15}$$

At all other boundary points no tracer mass leaves the domain, i. e.

$$\vec{j}^\alpha \cdot \vec{n} = 0, \quad \text{when} \quad \vec{v}\cdot\vec{n} = 0 \tag{16}$$

In the above equations (14) - (16), j_w^α denotes the inflow tracer mass flux at the boundary (wall), and c_w^α is the tracer concentration at the boundary. If sedimentation of tracers or their back solution into the water mass must be modelled, then j_w^α must also be prescribed along the bottom boundary. This however will not be our concern here.

This completes the formulation of the boundary conditions.

3. Numerics

The above system of differential equations for the velocity, temperature and tracer mass fields, paired with the corresponding boundary conditions have been numerically programmed. Since the

tracer concentrations are supposed to be so small, the density of the mixture is only negligibly affected by the presence of the tracer. Boundary conditions for the tracers are decoupled from those for the velocity and temperature fields, so the system can be decoupled and consecutively solved: first the equations for the velocity and temperature fields are solved and subsequently with their knowledge the tracer fields are determined.

To this end a semi-spectral model was designed with semi-implicit integration in time. The model is the semi-spectral model SPEM developed by Haidvogel *et al* (1991), and was extended by us to account for implicit temporal integration. In this model the variation of the field variables in the vertical direction is accounted for by a superposition of Chebyshev polynomials, but finite difference discretization is used in the horizontal direction. By using the so-called σ-transformation, the lake domain is transformated to a new domain with constant depth and this cylindrical region is yet again transformed in the horizontal coordinates by using conformal mapping which maps the shore as far as possible onto a rectangle. Theoretically such a mapping always exists, but in practice when discretizations are introduced, the emerging grid may become unjustifyably fine. In such cases the bounding line underlying the Schwarz-Chrystoffel transformation deviates in some segements from the actual shore line. This will be the case for Lake Constance.

We claim that our work is the first numerical application of diffusion problems with a semi-spectral model for a lake. Because of the small water depths of lakes in comparison to the ocean the original SPEM model had to be altered to permit economically justifyable time steps (SPEM uses explicit temporal integration, which, because of conditional numerical stability, requires small time steps). In Wang & Hutter (1998) several finite difference schemes, implicit in time, were introduced; that scheme which uses implicit integration in time in the vertical direction was the most successful one. The effectiveness of the proposed method is demonstrated by Wang (1996) and Wang & Hutter (1998).

In the previous work the diffusion equation was not incorporated. This is now done by using a leep frog procedure for integration in time, upstream differencing for the advective terms and central differences for the horizontal diffusive terms as follows:

$$\frac{\underbrace{c^{n+1}_{\alpha i,j}} - c^{n-1}_{\alpha i,j}}{2\Delta t} + u^n_{i,j}\frac{c^n_{\alpha i+1,j} - c^n_{\alpha i-1,j}}{2\Delta x} + |u^n_{i,j}|\frac{2c^n_{\alpha i-1,j} - c^n_{\alpha i+1,j} - c^n_{\alpha i-1,j}}{2\Delta x} +$$

$$v^n_{i,j}\frac{c^n_{\alpha i,j+1} - c^n_{\alpha i,j-1}}{2\Delta y} + |v^n_{i,j}|\frac{2c^n_{\alpha i,j} - c^n_{\alpha i,j+1} - c^n_{\alpha i,j-1}}{2\Delta y} + w^n_{i,j}\underbrace{\left(\frac{\partial c_\alpha}{\partial z}\right)^{n+1}_{i,j}} \tag{17}$$

$$= D^{c_\alpha}_H\frac{c^{n-1}_{\alpha i+1,j} - 2c^{n-1}_{\alpha i,j} + c^{n-1}_{\alpha i-1,j}}{\Delta x^2} + D^{c_\alpha}_H\frac{c^{n-1}_{\alpha i,j+1} - 2c^{n-1}_{\alpha i,j} + c^{n-1}_{\alpha i,j-1}}{\Delta y^2} + \underbrace{\left(\frac{\partial}{\partial z}(D^{c_\alpha}_V\frac{\partial c_\alpha}{\partial z}\right)^{n+1}_{i,j}}$$

In this equation lower case Latin subscripts (i, j) denote horizontal mesh points while upper case superscripts (n) indicate the time step. The two terms indicated by curly brackets represent vertical advection and diffusion; they are for simplicity here written prior to the application of the σ-transformation and are evaluated at the new, unknown time step. Because of the spectral expansion in the vertical, these terms need special handling when being discretized, see Wang & Hutter (1998). We show there that for each water column only a linear system of equations must be solved to advance the computation in time, a step that can quickly and unproblematically be solved.

4. Parameter selection

Computations were performed for a rectangle of extent 65× 10 km^2 and 100 m depth, and for Lake Constance, both under homogeneous, barotropic and stratified, baroclinic situations and exposed to external wind forcings. For both cases $L\times M = 65 \times 17$ mesh points were chosen in the horizontal direction amounting to a grid size of $\Delta x = \Delta y = 1$ km (exactly for the rectangle, variable and in the mean for Lake Constance).

In ensuing developments values of the diffusivities will be prescribed even though they ough to be computed according to the turbulence intensity present at a certain location of the wate body. This is done so here since the model is still in a phase of development where its proper performance is tested. Later applications ought to use algebraic Reynolds stress parameterization.

The diffusivities will be taken as follows:

(i) for homogeneous water:

$$\nu_H = 1.0\mathrm{m}^2\cdot\mathrm{s}^{-1},\quad \nu_V = 0.02\mathrm{m}^2\cdot\mathrm{s}^{-1},\quad D_H^{c_\alpha} = 1.0\ \ \mathrm{m}^2\cdot\mathrm{s}^{-1},\quad D_V^{c_\alpha} = 0.005\mathrm{m}^2\cdot\mathrm{s}^{-1} \tag{18}$$

(ii) for stratified water:

$$\nu_V = \begin{cases} 0.04, & z > -20\ \mathrm{m}, \\ 0.004, & -20\ \mathrm{m} \geq z \geq -40\ \mathrm{m}, \\ 0.02, & z < -40\ \mathrm{m}. \end{cases} \quad [\mathrm{m}^2\cdot\mathrm{s}^{-1}]'$$

$$\nu_H = 1.0\mathrm{m}^2\mathrm{s}^{-1},$$

$$D_V^{c_\alpha} = \begin{cases} 0.005, & z > -20\ \mathrm{m}, \\ 0.00005, & -20\ \mathrm{m} \geq z \geq -40\ \mathrm{m}, \\ 0.0005, & z < -40\ \mathrm{m}. \end{cases} \quad [\mathrm{m}^2\cdot\mathrm{s}^{-1}]' \tag{19}$$

$$D_H^{c_\alpha} = 1.0\mathrm{m}^2\mathrm{s}^{-1},$$

Except for the tracer diffusivities these choices were motivated and extensively discussed by Wang & Hutter (1998). It may suffice here to re-iterate that their choice is not entirely free, as it depends to a certain extent also on the numerical stability of the code. Thus, the number of Chebyshev polynomials must for homogeneous water be at least 12 and for stratified water 18 (see,

however, below) to perform stable computations with the above choices. Also, the initial stratification, from which baroclinic wind-induced currents are calculated, are of some (limited) influence.

For the rectangle the initial temperature distribution was taken to be

$$T(t=0) = \begin{cases} 17 - 2\exp(-(z+20)/5), & z \geq -20\,\mathrm{m}, \\ 5 + 10\exp((z+20)/20), & z < -20\,\mathrm{m}, \end{cases} \quad [^{o}C]. \tag{20}$$

It corresponds to a typical summer stratification of an alpine lake and is chosen in conformity with the diffusivities (19) to account for the fact that the vertical turbulent diffusivities must be much smaller in the thermocline than they are in the epilimnion and the hypolimnion.

Unfortunately, using the above parameterizations (19) and (20) no stable computations could be performed for stratified Lake Constance. This needed the initial temperature profile

$$T(t=0) = \begin{cases} 17 - 2\exp(-(z+10)/5), & z \geq -10\,\mathrm{m}, \\ 5 + 10\exp((z+10)/20), & z < -10\,\mathrm{m}, \end{cases} \quad [^{o}C], \tag{21}$$

(of which the largest vertical temperature gradient is slightly shifted upwards) and a somewhat larger turbulent vertical momentum exchange coefficient

$$\nu_V = \begin{cases} 0.04, & z > -20\,\mathrm{m}, \\ 0.01, & -20\,\mathrm{m} \geq z \geq -40\,\mathrm{m}, \\ 0.02, & z < -40\,\mathrm{m}. \end{cases} \quad [\mathrm{m}^2 \cdot \mathrm{s}^{-1}] \tag{22}$$

$$D_V^T = \begin{cases} 0.0005, & z > -20\,\mathrm{m}, \\ 0.0001, & -20\,\mathrm{m} \geq z \geq -40\,\mathrm{m}, \\ 0.0002, & z < -40\,\mathrm{m}. \end{cases} \quad [\mathrm{m}^2 \cdot \mathrm{s}^{-1}]$$

of course, numerical stability could be reached with even smaller vertical diffusivities, but they would require a larger number of Chebyshev polynomials and make computation time unduly long. The numerical values for the above diffusivities are realistic; Hutter (1984) has collected data by a number of authors taken between 1913 and 1978 and finds that horizontal tracer diffusivities in the epilimnion range from 0.5 to 1.0 $m^2 \cdot s^{-1}$. Newer measurements by Peeters (1994) indicate that they are between 0.02 - 0.3 $m^2 \cdot s^{-1}$ for several Alpine lakes. On the other hand, Maiss *et al* (1994 a) claim from measurements in Lake Constance that they are as large as 7-30 $m^2 \cdot s^{-1}$. We regard that 1.0 $m^2 \cdot s^{-1}$ is an acceptable mean value.

Vertical diffusivities inferred from observations (Hutter, 1984; Maiss *et al*, 1994 b) are all somewhat smaller; here computational times still set us a certain limit in the selection of the correct order of magnitudes. We claim them, however, to be more realistic than those in many other programs that have been used for lakes.

5. Tracer diffusion in a rectangular basin

We shall only present results pertinent to the diffusion of a tracer and not the velocity and temperature fields which evolve along with it. These have been amply scrutinized by Wang & Hutter (1998) for the wind scenarios used also here. The rectangular basin has dimension 65 ×17 km^2 ×100 m, a tracer flow of 20 $mg \cdot m^{-2} \cdot s^{-1}$ will be applied over an area of 1.0 ×1.0 km^2 in the middle

of the lake surface, commencing at t = 0 and abruptly terminating 24 hours later. Pure diffusion and diffusion with advection will be analysed.

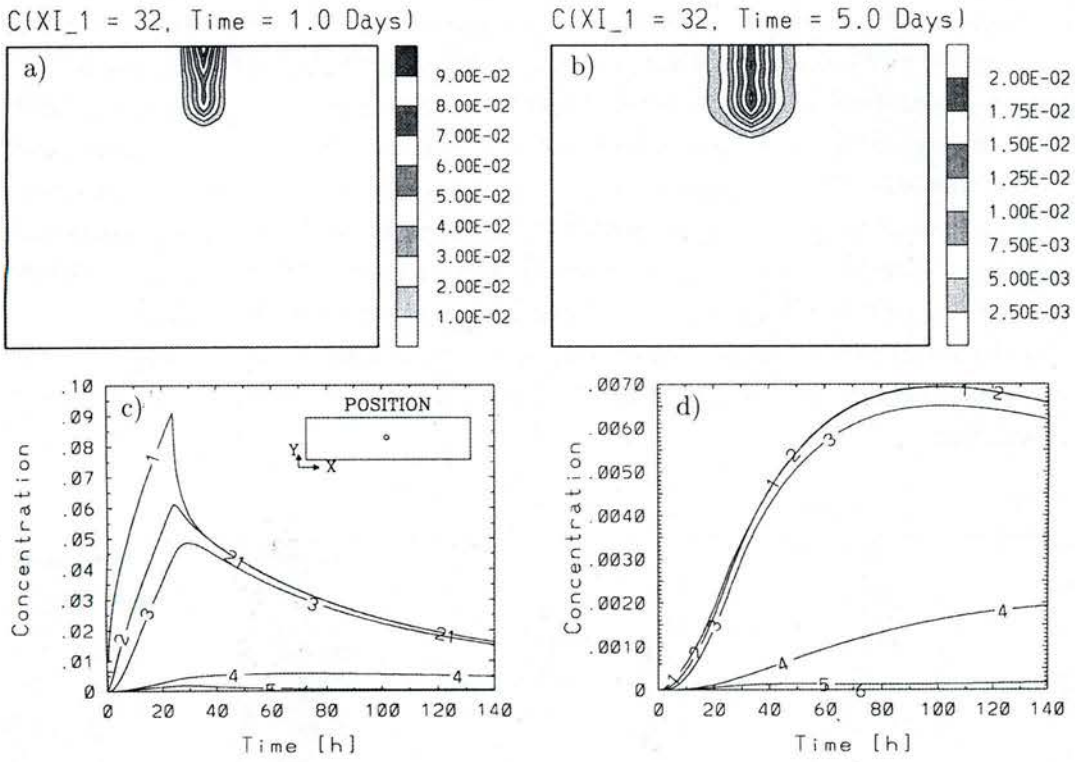

Fig. 1 Rectangular basin, homogeneous water

Isolines of the tracer concentration at the midlake south-north vertical cross section one day (a) and 5 days (b) after commencement of tracer inflow at the midlake position. Contours show concentrations in $mg \cdot m^{-3}$.

Time series of tracer concentration at 10 m depth intervals at midlake position (c) and a position 1 km distant (d) from it. The labels (1, 2, 3, ..., 11) correspond to the depths (0, 10, 20, ..., 100) m. Concentration is plotted in $[mg \cdot m^{-3}]$.

5.1 Pure diffusion

We ignore the application of any wind, suppose that the water is at rest throughout the basin but simultaneously assume that the turbulent eddy coefficients are acting as prescribed in section 4. Thus, the mean motion vanishes everywhere but the turbulent intensity is fully present. Such a situation might prevail after the cessation of a storm. Results are shown in Figs.1 - 2, pertinent for homogeneous and stratified waters, respectively. The top panels (a) and (b) in the two figures show vertical sections through the midpoint across the lake, i. e., a south-north section with isolines of the tracer concentrations one and five days after the flow of tracer into the lake began. As expected the tracer is in both cases symmetrically distributed; for a certain depth its concentration is maximum at the midlake position. For the homogeneous lake the tracer reaches the bot-

tom well before five days. During summer time the stratification with its strong thermocline prevents diffusion of tracer mass from the epilimnion to the hypolimnion. A tracer, released at the free surface can hardly be discerned in the hypolimnion. Panels (c) and (d) of Figs.1 and 2 show time series over 120 hours of the concentration at the depths 0, 10, 20, ..., 100 m (labelled by 1, 2, 3,..., 11) in a vertical line at the midlake position (panels c) and 1 km apart from it (panels d) for homogeneous and stratified waters. For the former the concentration at the free surface (label 1) increases sharply and monotonically as long as the tracer inflow continues (for 24 hours); after cessation of this inflow it drops quasi-exponentially in time. With increasing depth the maximum not only decreases, it simultaneously is shifted to larger times. For the position 1 km distant from the lake center (panels d), this maximum at the free surface is reached about 30 hours after the cessation of the tracer inflow, and it is further shifted to larger times for larger depths. Obviously the absolute values of the concentration are also smaller by a factor of approximately 30. Comparing the concentration-time series of Fig. 1 at various depths, it becomes clear that a smooth decay with time

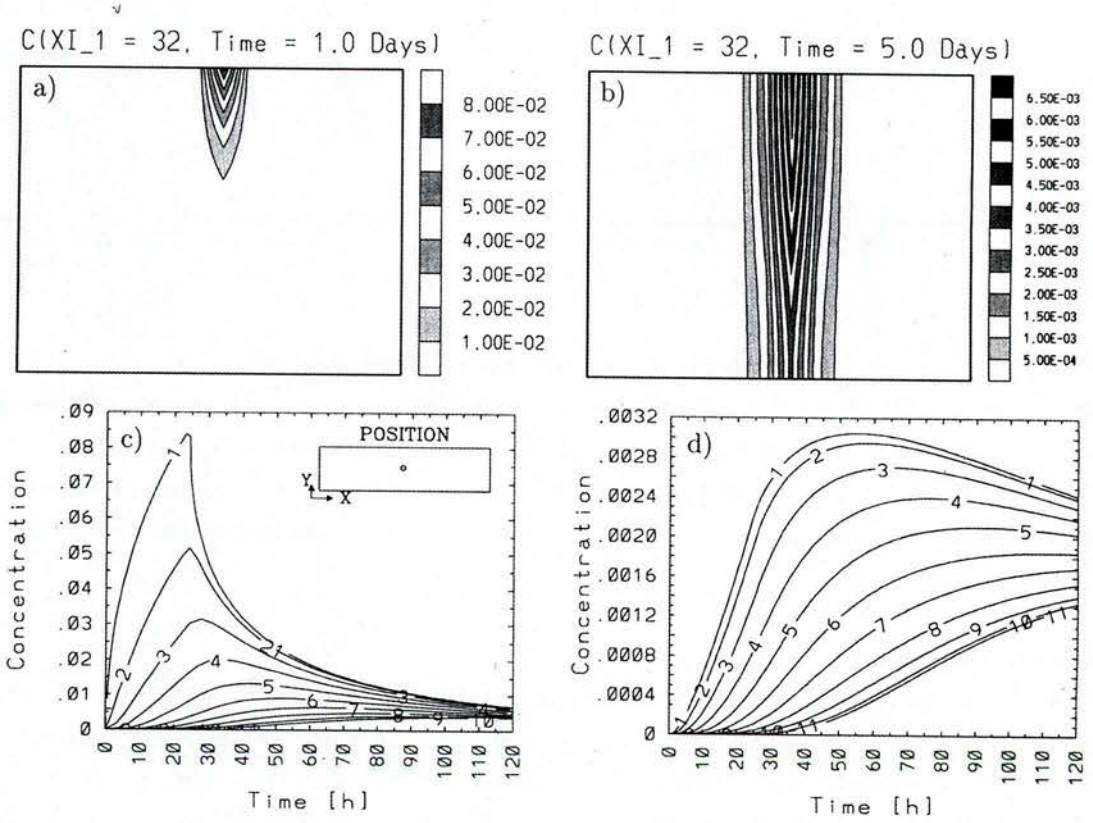

Fig.2 Rectangular basin, stratified water

Isolines of the tracer concentration at the midlake position, (a) and (b), and time series of tracer concentration at 10 m depth intervals at the midlake position (c) and 1 km distant from it (d).For further details, see also caption to Fig.1

and depth is reached. This is quite different for stratified water, see Figs. 2 c,d. Here, concentration-time series indicate that the tracer stays essentially in the upper 20 m as isolines at 30 m depth and deeper indicate much lower concentration values than above. Interesting is also the fact that the concentration in the epilimnion, 1 km distant from the lake center, is practically uniform and only changes with time. Here the concentration maximum at the free surface is reached about 75 hours after the cessation of the tracer inflow. Absolute values for the concentration are about twice as large as for the homogeneous lake.

5.2 Diffusion and advection

Diffusion of a tracer is substantially increased if advection by a mean turbulent velocity field is present; it is generated here by a wind exerted in the long direction of the basin (from west to east). The wind stress applied is τ_0=0.05 N·m^{-2} which corresponds to a wind speed of 4.7 m·s^{-1} (a low to medium size storm). This wind is impulsively applied at time t = 0 uniformly distributed over the free surface and lasts indefinitely for homogeneous water and 48 hours for stratified water. We discuss results obtained for homogeneous and stratified waters separately.

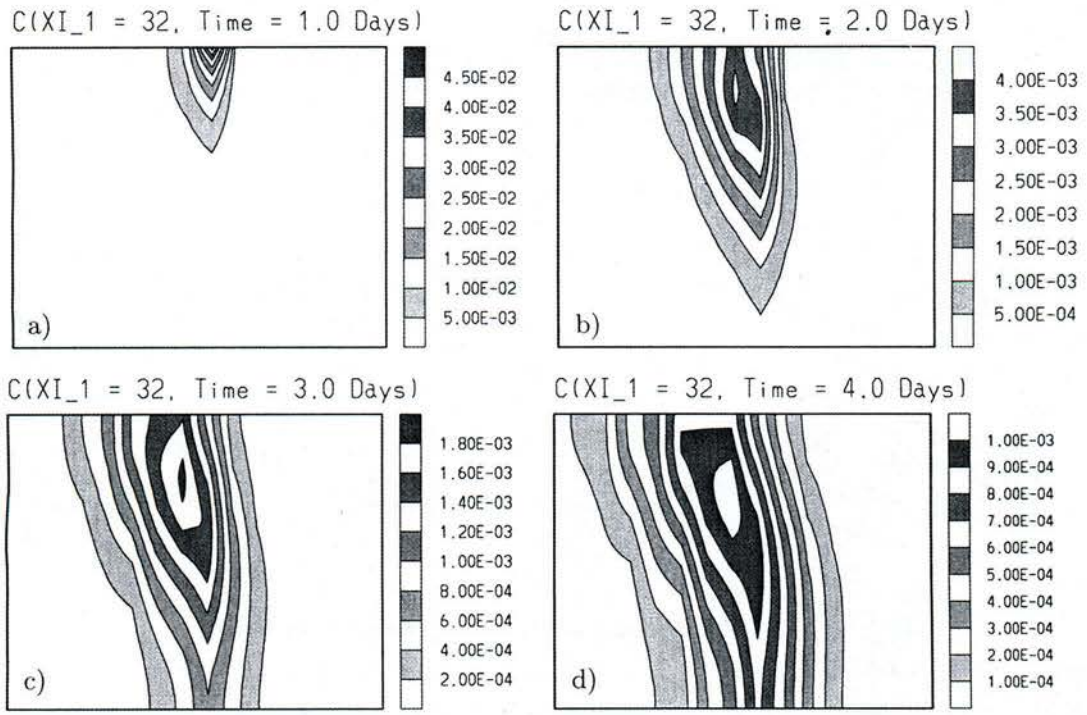

Fig. 3 Homogeneous water

Isolines of the tracer concentration in the south-north cross section through the lake center for an impulsively applied spatially uniform wind from west. Panels (a), (b), (c), (d) are for a time 1, 2, 3, 4 days after the wind set-in and the tracer was released at the surface. The wind lasts forever and the tracer inflow at the midlake position is 20 mg·m^{-2}·s^{-1} on an area of 1.0 km^2 during the first 24 hours.

5.2.1 Homogeneous water

Fig.3 shows isolines for the tracer concentration in a midlake south-north cross section 1, 2, 3 and 4 days after the wind set-in. Owing to the Coriolis force the current in this cross section is towards south in the upper layer and towards north in the lower larger. The symmetry of the tracer distribution is therefore destroyed.

Because of the relatively large currents on the free surface the maximum concentration slowly moves from the free surface (at time t = 0) downwards; the horizontal spreading of the tracer is very fast as can be seen from the absolute values of the concentrations.

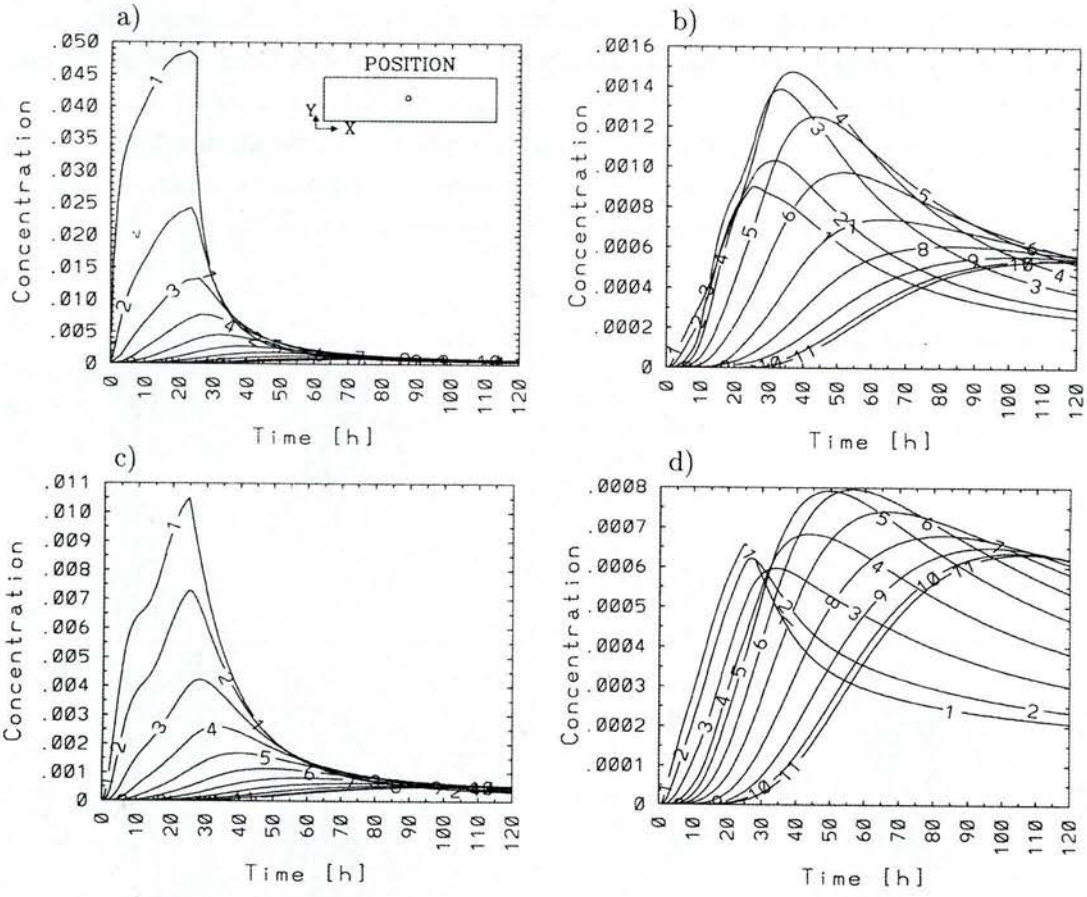

Fig. 4 Rectangular basin, homogenous water

Time series of the tracer concentration at the midlake position (a) and positions shifted 1 km from the lake center towards west (b), east (c) and north (d) for different depths. The labels (1, 2, 3, ..., 11) indicate points (0, 10, 20, ..., 100) m below the surface.

Fig.4 shows time series over 120 hours of the tracer concentration at various depths at the midlake position (panel a) and shifted towards west (b), east (c) and north (d), the labels (1, 2, 3, ..., 11) indicating depths (0, 10, 20, ..., 100) m. The tracer concentration at the midlake position at

first increases very rapidly, reaches at the free surface a maximum after 24 hours and thereafter drops very quickly to very low values. At lower depths this maximum is much smaller and also later reached. At the position 1 km downstream (panel c) the behaviour is principally the same with a small delay when the maximum is reached and somewhat smaller values for the concentration. In the upstream positions, on the other hand (panels b, d), the concentration reaches its maximum only some time after the cessation of the tracer inflow. The maximum concentration does not occur at the free surface, but at a medium depth; in addition, the absolute values of the concentrations at the upstream positions are considerably (more than 10 times) smaller than at the downstream positions.

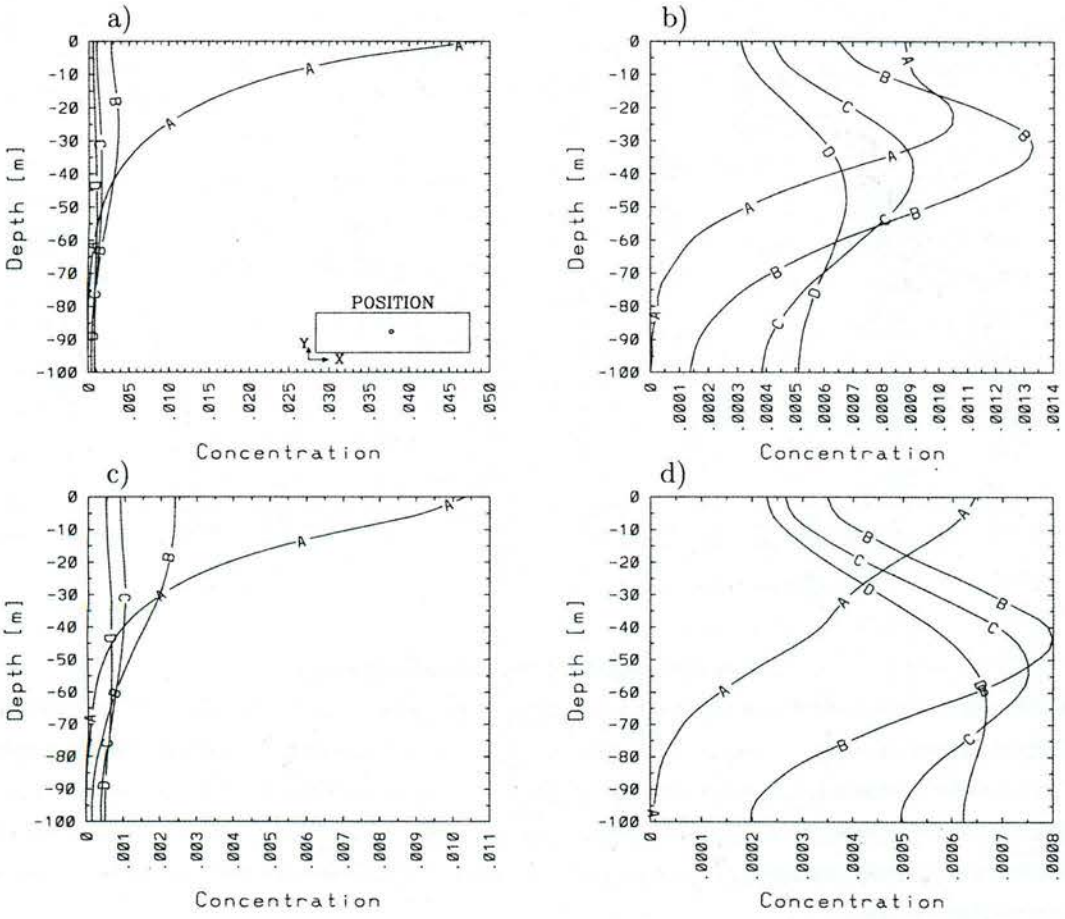

Fig. 5 Rectangular basin, homogeneous water

Vertical profiles of the concentration of a tracer for an impulsively applied spatially uniform wind from west and a concentration released on the free surface over a 1 km^2 area at the midlake position for 1 day. Curves labelled A, B, C, D give the conentration 1, 2, 3, 4, days after the inception of the experiment, and the panels are for the midlake position (a) and positions 1 km shifted from the middle towards west (b), east (c) and north (d). Note that the absolute values of the concentrations in upstream positions (panels b, d) are considerably smaller than in down-

stream positions (panels a, c).

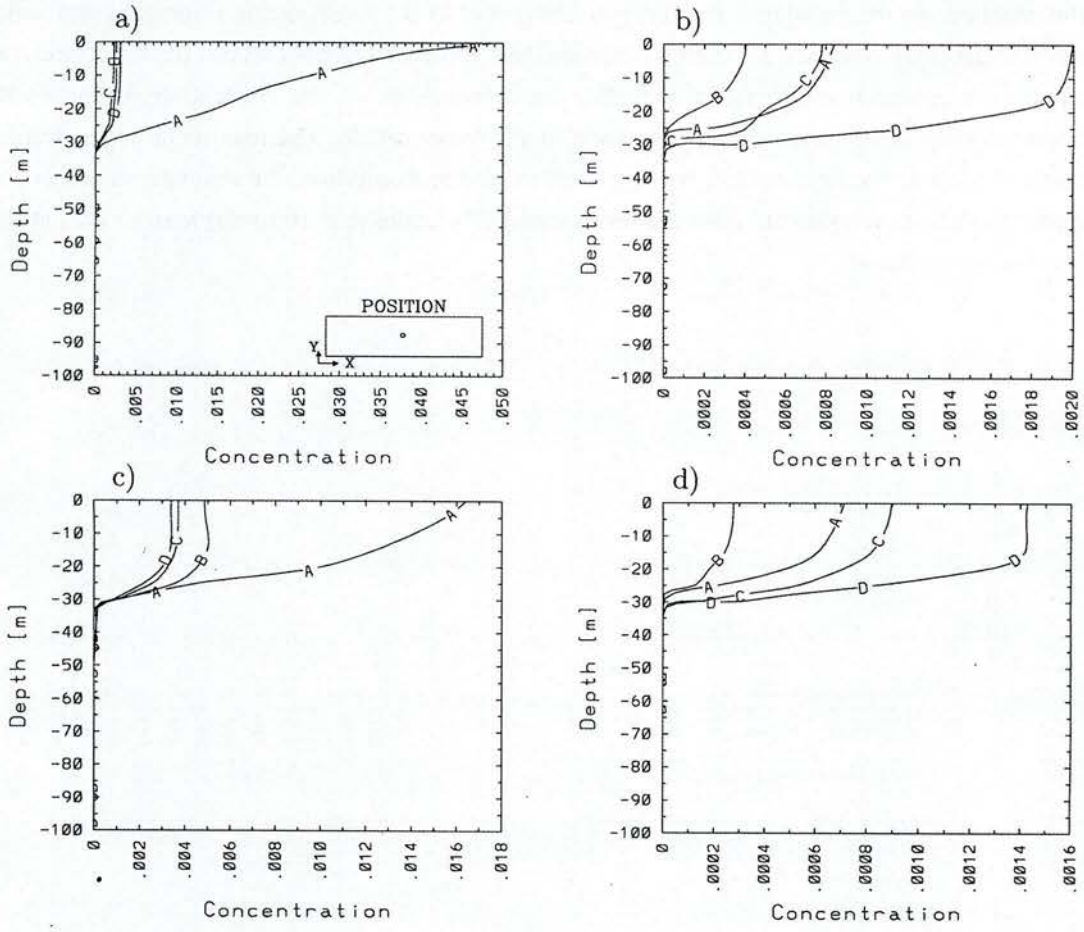

Fig. 6 Rectangular basin, stratified water

Vertical profiles of the concentration of a tracer for an impulsively applied spatially uniform wind from west and a concentration released on the free surface over a 1km^2 area at the midlake position for 1 day. Curves labelled A, B, C, D give the conentration 1, 2, 3, 4, days after the inception of the experiment, and the panels are for the midlake position (a) and positions 1 km shifted from the middle towards west (b), east (c) and north (d). Note that the absolute values of the concentrations in upstream positions (panels b, d) are considerably smaller than in downstream positions (panels a, c).

Interesting is also the information that can be deduced from vertical concentration profiles at the same locations as in Fig. 4. Such profiles are shown in Fig.5. It shows snapshots for these profiles one day (curves labelled (A)), two (B), three (C) and four (D) days after the wind set-up. The shifting of the maximum concentration to larger depths can clearly be seen at all four positions. As before, the concentrations at upstream positions (panels b, c) are much smaller than at down-

stream position (panel c). Parenthetically we also mention that upstream finite differencing for the advection is very important. Had we used central differences for the horizontal advective terms, then

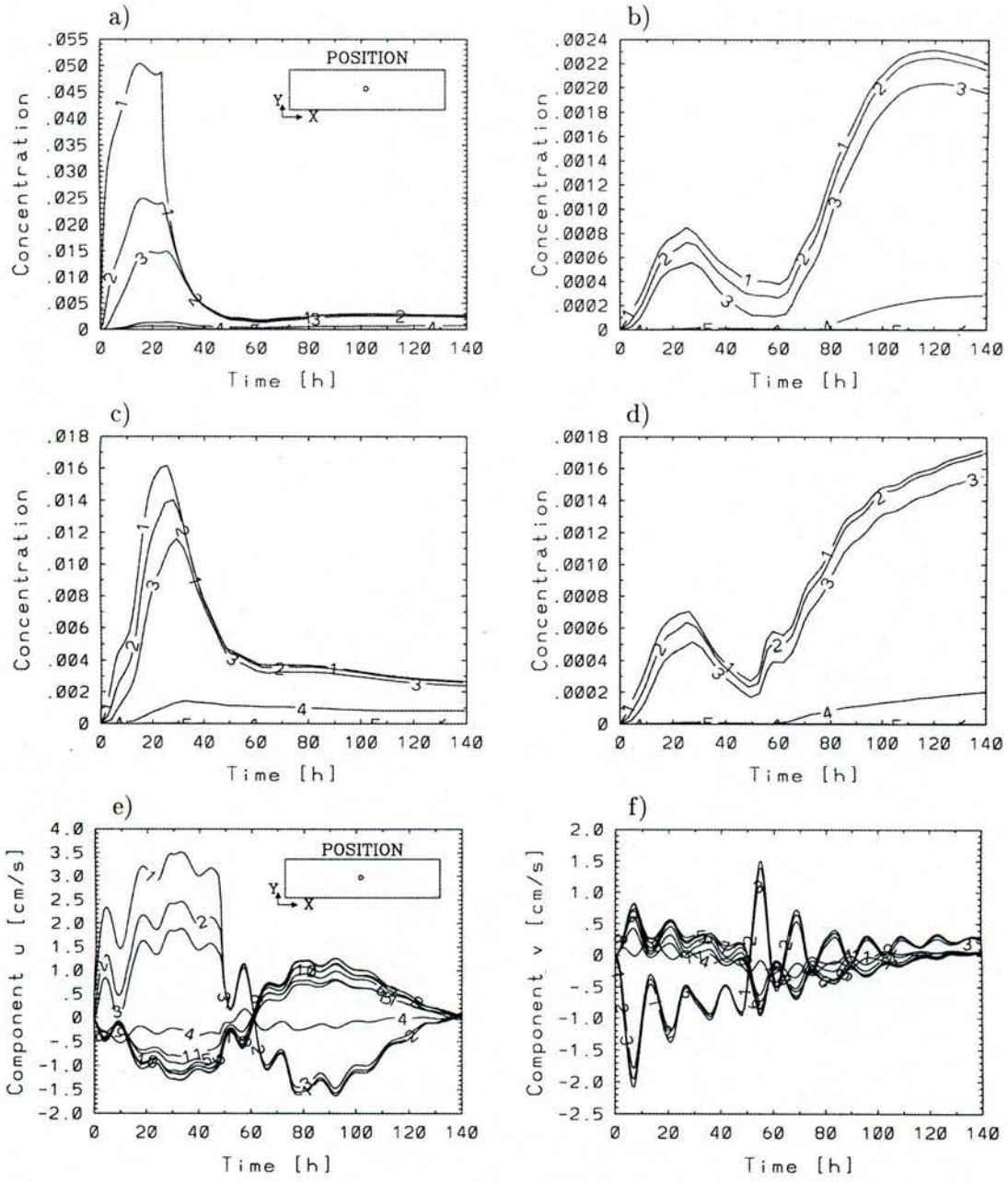

Fig.7 Rectangular basin, stratified water

Time series of the tracer concentration at the midlake position (a) and positions shifted 1 km from the lake center towards west (b), east (c) and north (d) for different depths. The labels (1, 2, 3, ..., 6) indicate points (0, 10, 20, ..., 50) m below the surface. Further, time series of the velocity components in the long (e) and transverse direction (f) at the midlake, position at the depths (0, 10, 20, ..., 100) m labelled by 1, 2, 3, ..., 11.

unphysical, negative concentrations would have been obtained in these cases at the upstream positions of Fig.5 b, d. That such unphysical results are avoided alltogether is one corroboration for the adequacy of our integration routine.

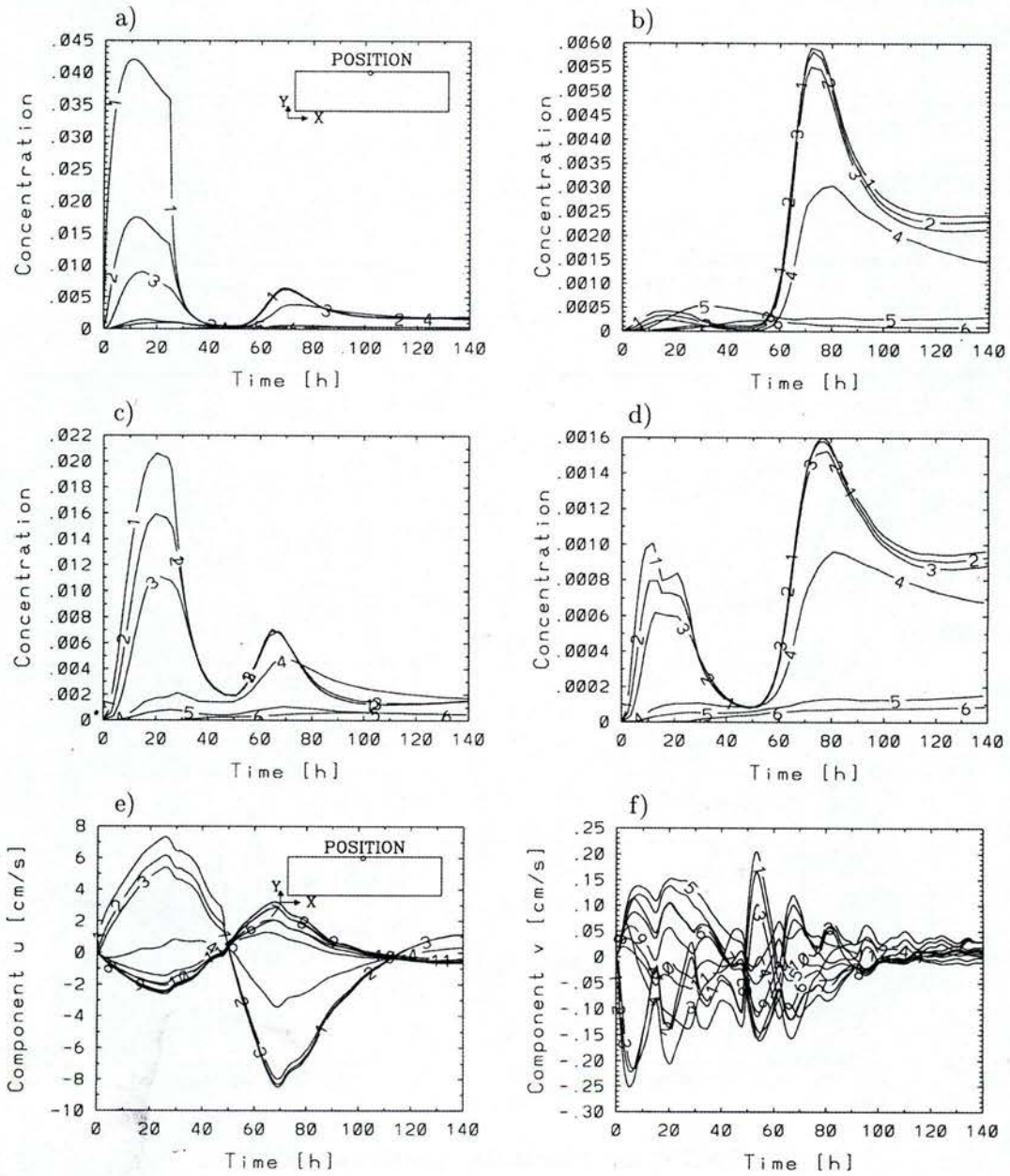

Fig. 8 Rectangular basin, stratified water

Time series of the tracer concentration for near shore positions at a point 500 m off-shore from the midpoint of the northern shore (panel a), 1 km west (b), east (e) and south (d) of it. Here a tracer flow of 20 $mg \cdot m^{-2} \cdot s^{-1}$ is applied

over an area of 1.0×1.0 km^2 near the midpoint of the northern shore. Shown are also the longitudinal (e) and transverse (f) horizontal velocity components. The labels (1, 2, 3, ..., 11) correspond to the depths (0, 10, 20, ..., 100 m).

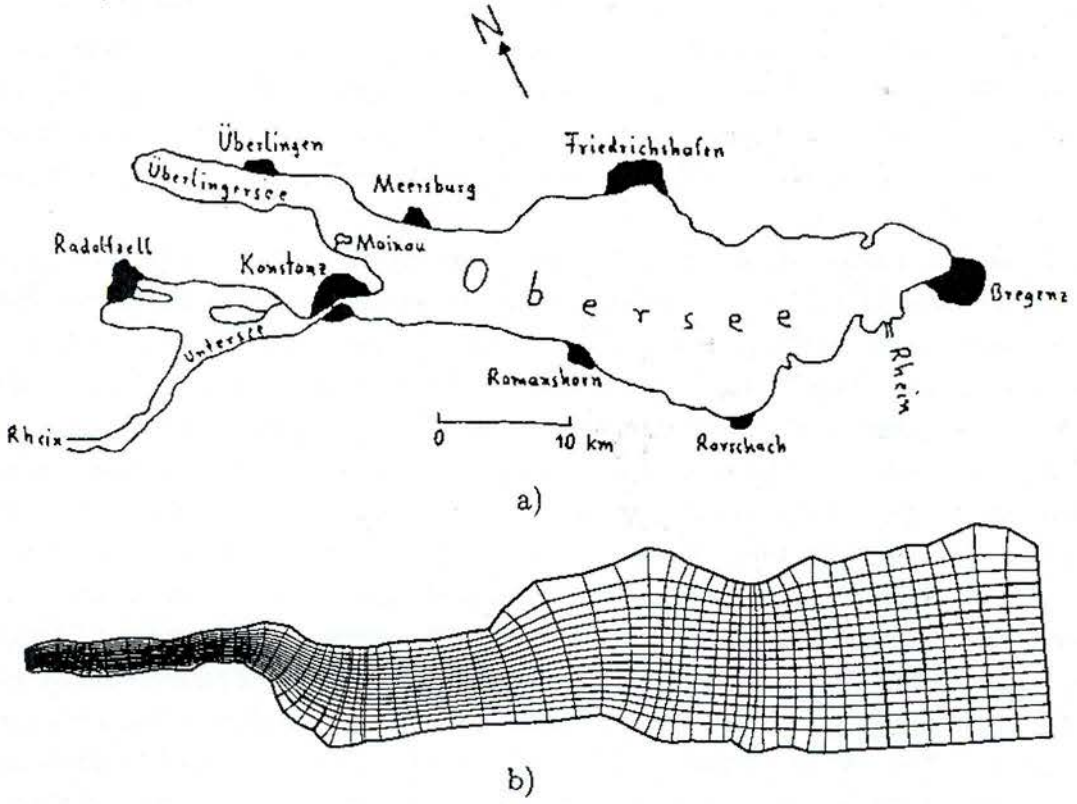

Fig. 9

a) *Map of Lake* Constance with bathymetry and a few towns indicated along its shore. Three basins characterize the lake: Obersee, Überlinger See and Untersee. b) Coordinate net for the Obersee and the Überlinger See with the "computational" shore line indicated as thick line.

5.2.2 Stratified water

The scenario for the applied wind and the inflow of the tracer will be the same as before but the wind will abruptly stop after two days. The initial temperature distribution will be chosen according to (20), and the diffusivities are selected as stated in (19). Fig.6 corresponds exactly to Fig.5, but holds now for the stratified basin. It is obvious that the concentration is confined to the top 30 metres (i.e., the epilimnion) with virtually no diffusion through the thermocline. Concentration maxima essentially occur at the free surface (with an insignificant exception in Fig.6 c, curves B, C, D). Moreover, as time proceeds from 1 to 4 days the concentration on the upper layer is increasingly homogenized. Very interesting, and especially informative when being compared with results of Fig. 4 are the time series of the concentration displayed in Fig. 7 (a) - (d). The time

evolution of the tracer concentrations at the four positions (lake center, and 1 km to the west, east and north) shows conspicuous oscillations. In particular, west and north of the midlake position the concentration reaches far larger values after the cessation of the wind than before; this is obviously the effect of the backward swing of the water after the cessation of the wind. This backward swing is due to baroclinic Kelvin-type oscillations. The reader can convince himself of this conjecture by comparing the time series of the tracer concentrations in Fig. 7 b, d with the corresponding time series of the velocity components at various depths of the lake center in the long and transverse directions, respectively (Fig. 7 e, f). Both Kelvin and Poincarve-type oscillations are discernible. In the time series for the concentration the first can be clearly seen, the second only slightly.

A much more distinct signal of the Kelvin-type oscillations in the time series of the concentrations can be discerned if the results plotted in Fig. 7 are repeated in Fig.8 for a near-shore position. But now a tracer flow of $20mg \cdot m^{-2} \cdot s^{-1}$ is applied over an area of 1.0×1.0 km^2 near the midpoint of the northern shore. Here the Kelvin-type oscillations have substantially larger amplitudes than at the midlake position, implying that the contribution of the advection to the tracer dispersion must also be correspondingly larger. Fig. 8 shows for a position 500 m off the northern shore (panel a) and 1 km west (b), east (c) and south (d) of it, time series of the tracer concentration at 10 m depth intervals. Because of the strong shore parallel currents towards east close to the border almost no than 50 hours. Then,concentration of tracer mass is reaching at the position shifted towards the west (panel b) for more after the cessation of the wind the concentration rapidly rises to a maximum reached after about 72 hours and due to the strong backward swing of the near shore current, after which the concentration is tapering off. At all other positions, two maxima are reached in the upper layer (above the 20 m depth) which coincide with the maximum and minimum of the upper layer shore parallel currents, corroborating the conjecture that advection is responsible as a cause. Interesting is also the fact that the time series of the tracer concentration at the 30 m depth level (labelled 4) also assumes appreciable values which is contrary to results obtained at the midlake position (see Fig. 7, curves labelled 4). This is a consequence of the strong downwelling at the northern shore that sets in after the cessation of the wind. It also appears to be clear that the Poincaré-type oscillations are not seen in the concentration-time series because its amplitudes in the transverse velocities are too small to generate a visible advective effect in the concentrations (compare Fig. 8 e and 7 e).

6. Tracer diffusion in Lake Constance

Fig. 9a shows a map of Lake Constance with a few of the larger towns situated along its shore and bathymetric lines indicating its depth. This Alpine lake borders Austria, Germany and Switzerland and consists of three basins: the large Obersee, Überlinger See and Untersee. The latter is dynamically discounected from the others by the 5 km long "Seerhein", the exit river of the two other basins. Obersee and Überlinger See are 64 km long and have a mean width of about 10 km. The Überlinger See is relatively shallow (~ 147 m deep) when compared with the 252 m

deep Obersee and somewhat separated from the latter by a sill north of the island Mainau. The mean depths are 79 and 101 m respectively. Fig. 9b also shows the curvilinear coordinate system

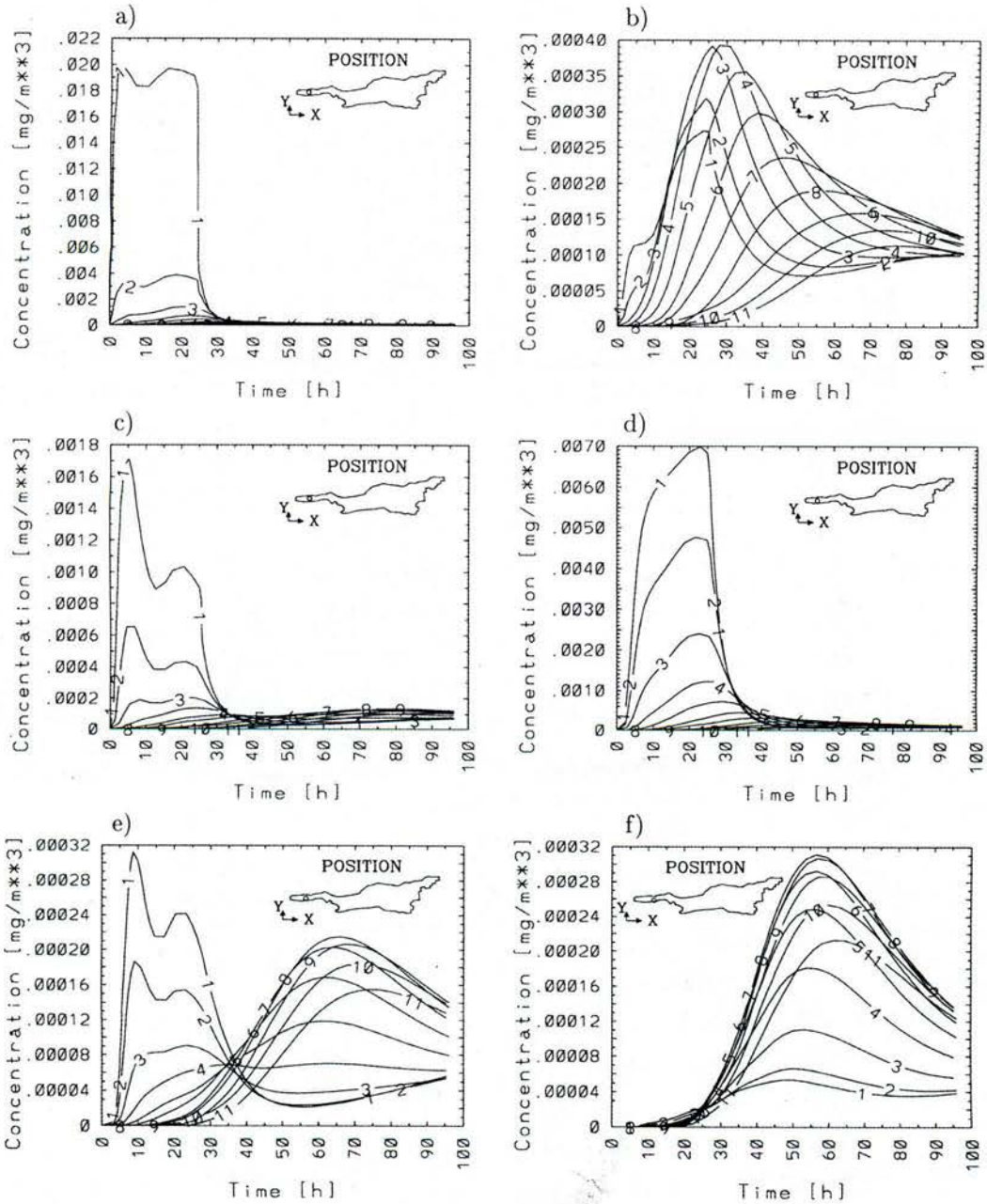

Fig. 10 Homogeneous Lake Constance

Time series of the tracer concentration at the position in the middle of theÜberlinger See (indicated by a circle in the inset map): at the center of the input area (a), 720 m west of it (b), 740 m east of it (c), 280 m south of it (d),

1.5 km southeast of it (e) and 3.2 km southeast of it (f). The curves show tracer concentrations as functions of time at various depths, the labels (1, 2, 3, ..., 11) indicating depths of (0, 10, 20, ..., 100) m. The tracer is released on a surface area of 730×times 140 m^2 in the middle of Überlinger See, about 5 km from its western most end with a strength of 20 $mg \cdot m^{-2} \cdot s^{-1}$ during the first 24 hours.

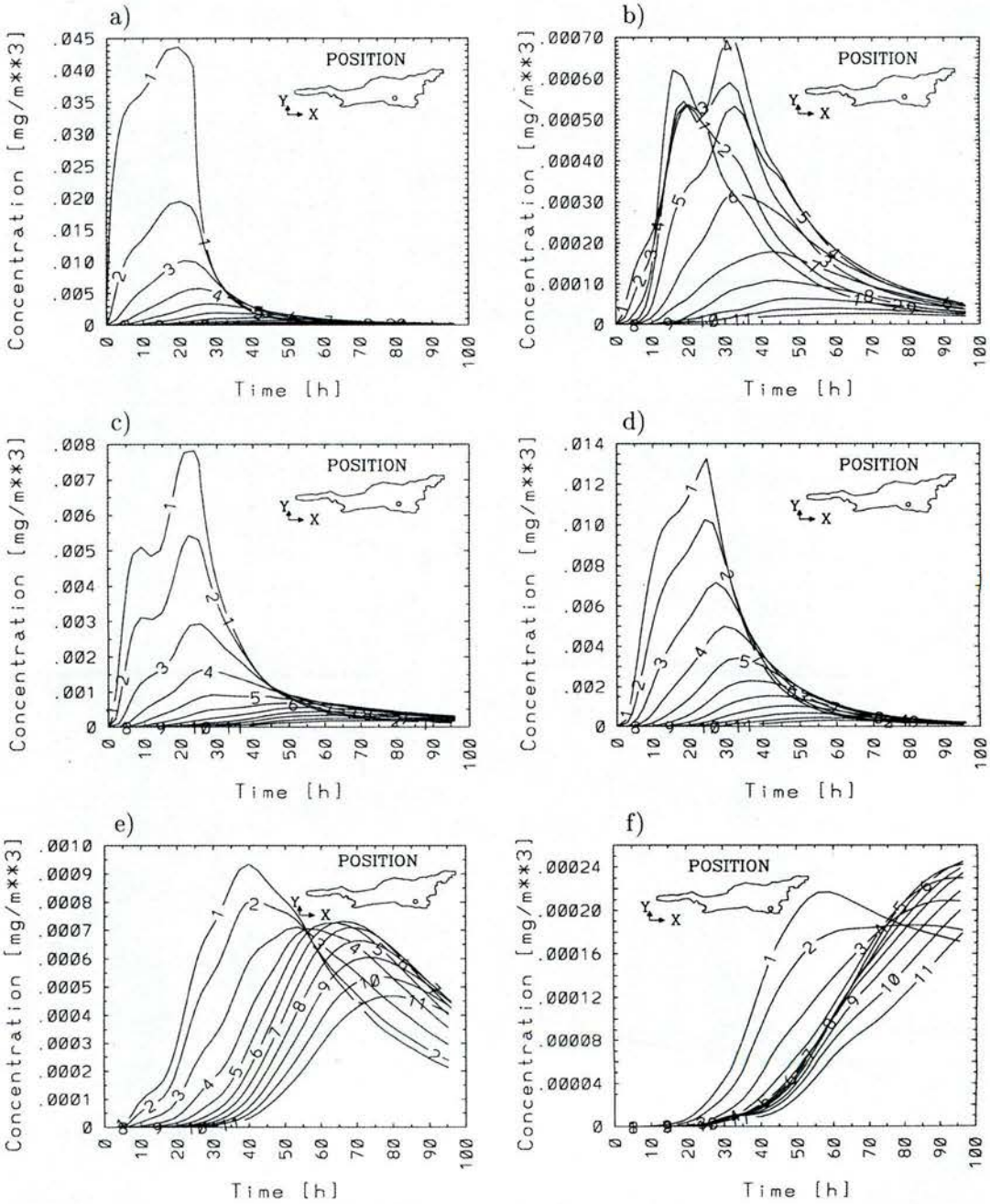

Fig. 11 Homogeneous Lake Constance

Same as Fig.~10 but for a position of the Obersee at a position 3 km north of the southern shore between Romanshorn and Arbon as indicated in the inset map: At the center of the tracer input area (a), 1.2 km west of it (b), 1.2 km east of it (c), 700 m south of it (d), 3.5 km towards south east (e), 5.3 km towards southeast (f). The tracer input area is 1 200 ×520 m^2 and the tracer mass flux 20 $mg \cdot m^{-2} \cdot s^{-1}$ during the first 24 hours.

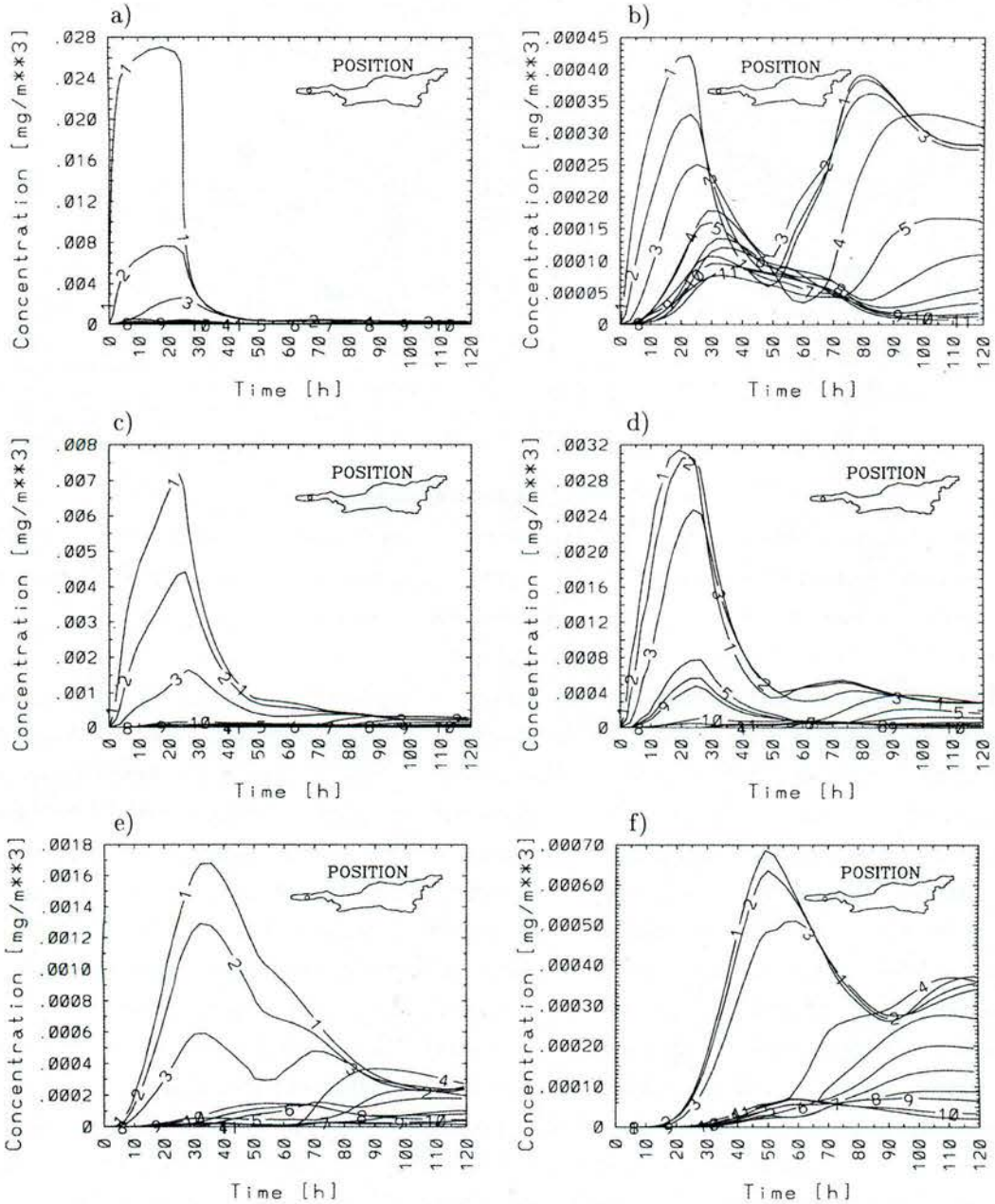

Fig. 12 Straified Lake Constance

Time series of the tracer concentration at the position in the middle of the Überlinger See (indicated by a circle in the inset map): at the center of the input area (a), 720 m west of it (b), 740 m east of it (c), 280 m south of it (d),

1.5 km southeast of it (e) and 3.2 km southeast of it (f). The curves show tracer concentrations as functions of time at various depths, the labels (1, 2, 3, ..., 11) indicating depths of (0, 10, 20, ..., 100) m. The tracer is released on a surface area of 730 × 140 m^2 in the middle of Überlinger See, about 5 km from its western most end with a strength of 20 $mg \cdot m^{-2} \cdot s^{-1}$ during the first 24 hours.

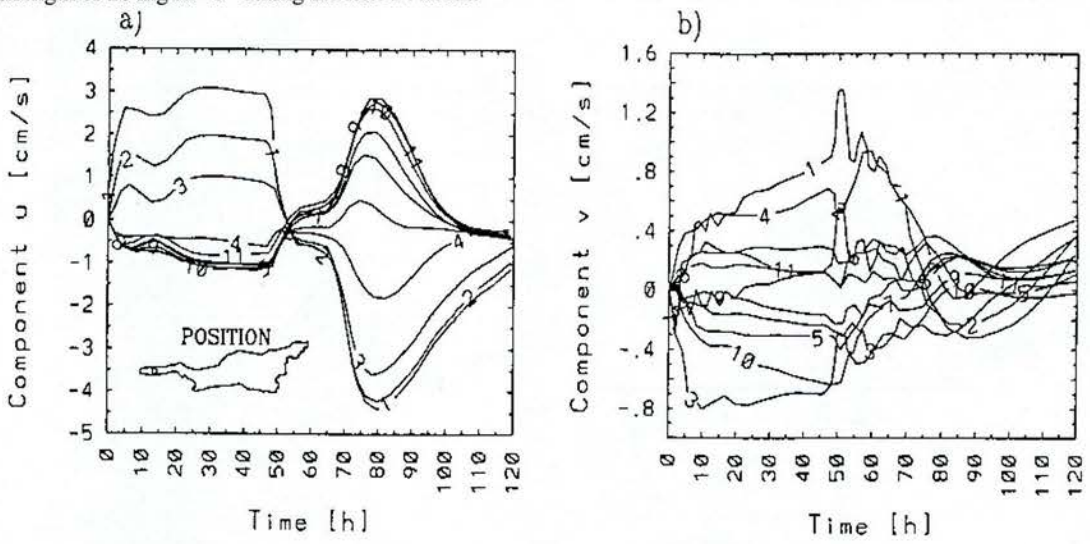

Fig. 13 Stratified Lake Constance

Time series of the horizontal velocity components in the *x* and *y*-directions (a, b) at a midpoint of Überlinger See (approximately 5 km from its western end) for various depths and a wind blowing 305° from True NW during two days uniformly over the lake. The labels (1, 2, 3, ..., 11) correspond to the (0, 10, 20, ..., 100) m depths.

6.1 Homogeneous Lake Constance

Here we demonstrate that, qualitatively, the results are very similar to those obtained with the rectangular basin with constant depth; additional features enter because of the topographically induced motions. The impulsively applied wind is spatially uniform and blows from 305° True NW; it corresponds to a wind acting in the long direction of the lake; its strength is t = 0.05 $N \cdot m^{-2}$, corresponding to a windspeed of 4.7 $m \cdot s^{-1}$. The tracer is released at the free surface of the lake, once in the middle of Überlinger See, 5 km off-shore from its western end, on an area of approximately 730×140 m^2, once in the Obersee, 3 km from the southern shore between Romanshorn and Arbon on an area of approximately 670×610 m^2; in both cases a flow density of 20 $mg \cdot m^{-2} \cdot s^{-1}$ is applied during one day after which the inflow is shut-off. The time series of the tracer concentra tions for the two cases are shown in Figs. 10 and 11 for the central point of the input area and five neighbouring points as described in the figure captions. In the Überlinger See, at the center of the tracer input area, the tracer concentration increases sharply shortly after the commencement of the input and then stays more or less constant for approximately 24 hours when it drops again to negligible values within only a few hours. At the 10 m depth level the concentration is about a factor of five smaller, and at 20 metres and below it is negligible. Very small, Coriolis-force induced oscillations are also visible, but these are stronger at positions east and southeast of the source (see

more, that at medium to large depths the concentration increases considerably both at upstream (panel b) and downstream (panels e, f) locations, that the onset of this sharp increase is at the downstream positions delayed by approximately one day (panels e, f) but reaches the upstream position somewhat earlier (panels b). The absolute values of the concentration reached here are considerably larger than at the free surface.

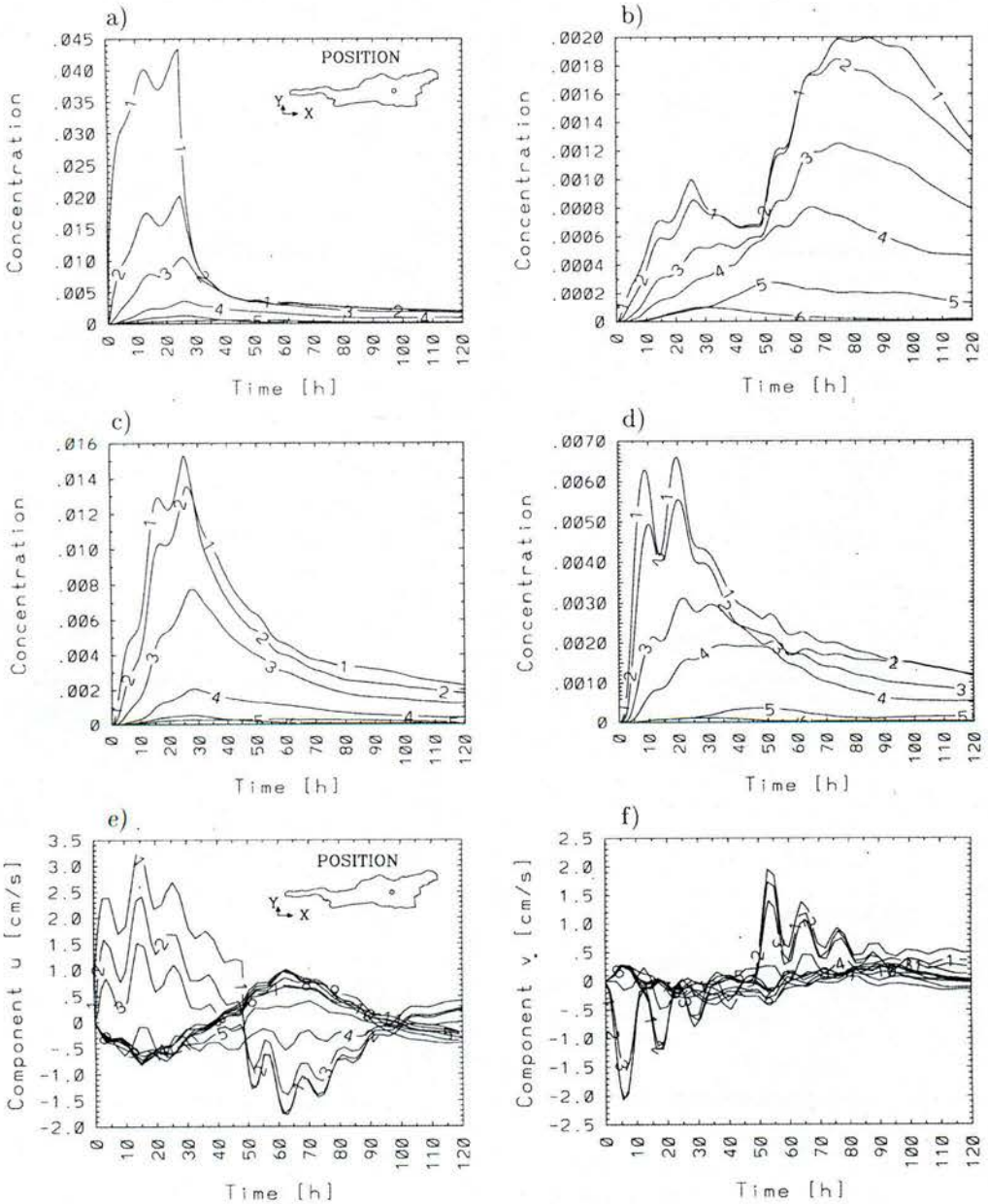

Fig. 14 Stratified Lake Constance

Time series of the tracer concentration at a midlake position in the Obersee, (a), 700 m west of it (b), 700 m east of it (c) and 600 m south of it. Panels (e) and (f) show the components of velocity in the x-direction (e) and y-direction (f). The wind from 305° True NW is uniformly distributed over the lake, has strength 0.05 Nm^{-2} (4.7 ms^{-1})

and suddenly stops after 24 hours. The tracer input is on the free surface on an area of 670× 610 m^2 and possesses a strength of 20 $mg \cdot m^{-2} \cdot s^{-1}$. The labels (1, 2, 3,..., 11) denote depths of (0, 10, 20,..., 100 m).

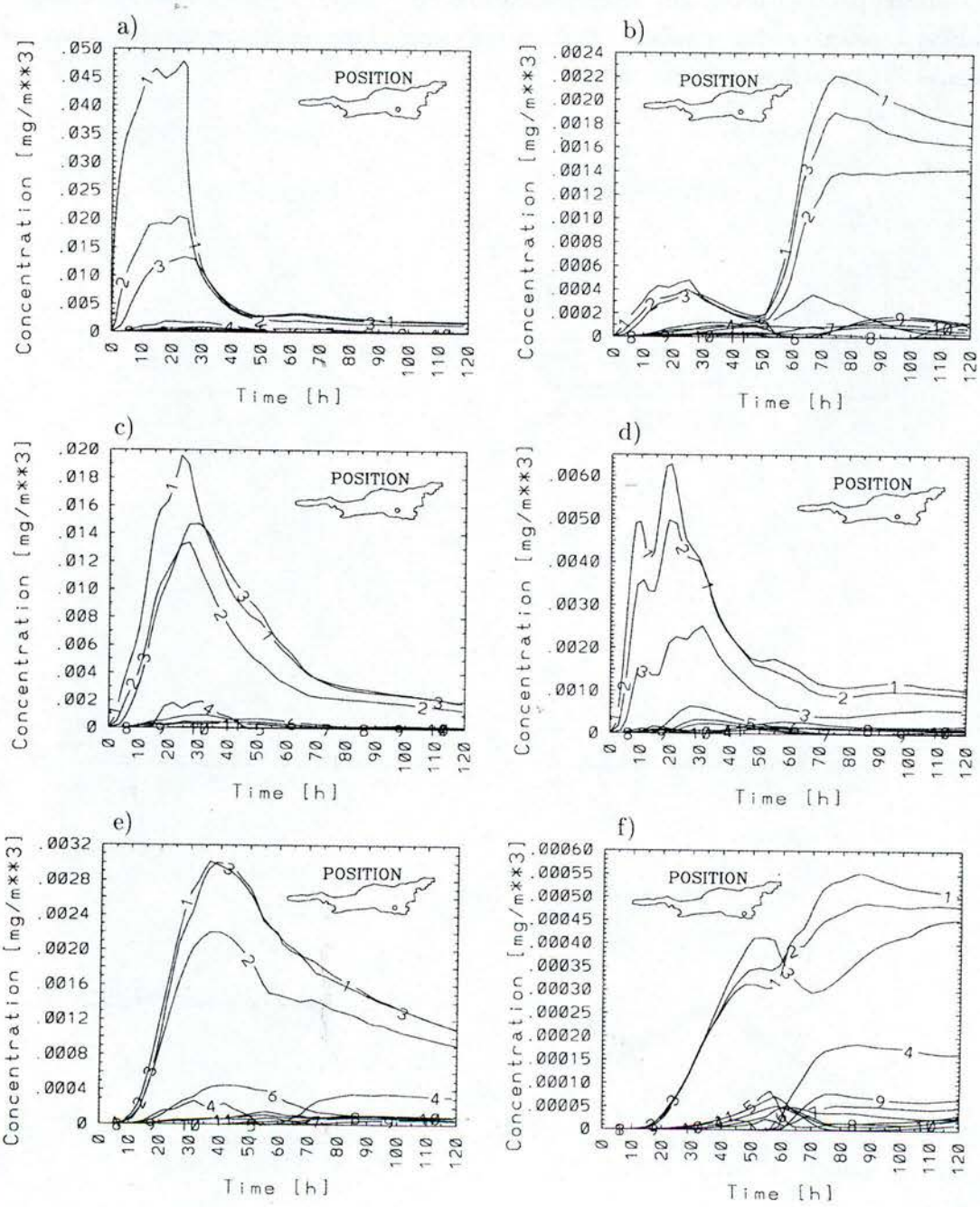

Fig. 15 Stratified Lake Constance

Same as Fig. 11. Time series of the tracer concentration for a position of the Obersee at a position 3 km north of the southern shore between Romanshorn and Arbon as indicated in the inset map: At the center of the tracer input

area (a), 1.2 km west of it (b), 1.2 km east of it (c), 700 m south of it (d), 3.5 km towards south east (e), 5.3 km towards southeast (f). The tracer input area is 1 200 ×520 m^2 and the tracer mass flux 20 $mg \cdot m^{-2} \cdot s^{-1}$ during the first 24 hours.

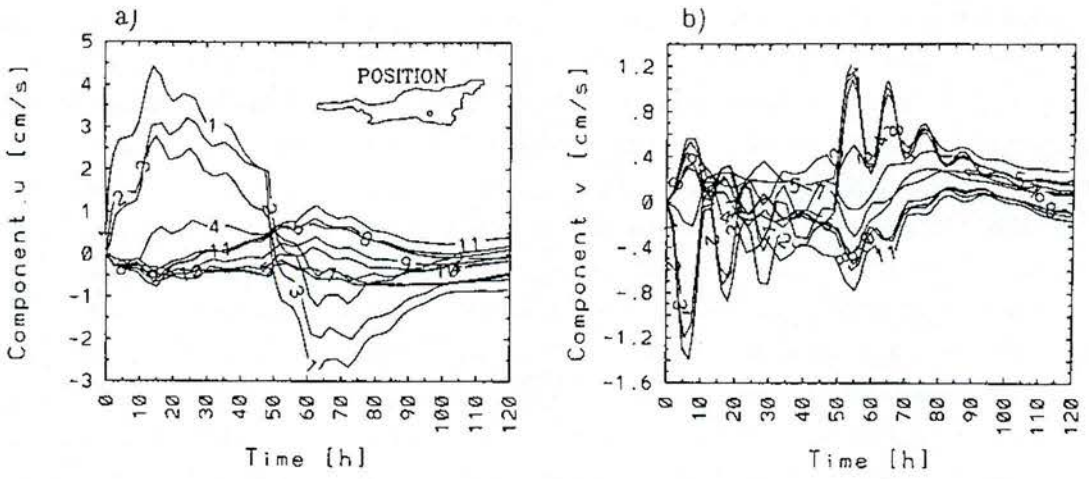

Fig. 16 Stratified Lake Constance

Time series of the horizontal velocity components at the central position (same as in Fig. 15 (a) of the tracer input app. 3 km off-coast from Romanshorn-Arbon for various depths. The labels (1, 2, 3, ..., 11) indicate the depths (0, 10, 20, ..., 100) m.

Fig. 11 shows the analogous results obtained for a tracer dispersion experiment in the Obersee as described in the figure caption. The results are qualitatively very similar to those obtained for the Überlinger See with the exception that here the upper layer concentrations, in particular at the surface are largest (except panel f). However, traces of the inertial oscillation can also be seen (panels b, c).

To sum up, in homogeneous water, a tracer entering the lake through the free surface will quickly spread both horizontally and vertically and maximum concentrations will after 4 days have decreased to values below1% of the initial concentrations.

6.2 Stratified Lake Constance

Results for the stratified Lake Constance are considerably different. Appreciable values for the concentration are now essentially restricted to the epilimnion, inertial waves are not visible, but depending on the location more or less clear tracer of Kelvin- and Poincaré-type waves can be seen. We shall employ the same wind scenario from 305°True NW uniformly applied for two days after which the wind abruptly stops; its strength is again T=0.05 $N \cdot m^{-2}$ or 4.7 $m \cdot s^{-1}$. The tracer input is per formed as it was done for the homogeneous lake.

Fig. 12 corresponds to Fig. 10 and displays the time series of the tracer concentrations at the positions as described in the figure captions.In the central position of the tracer input area (a) the tracer concentration rapidly grows and reaches almost a maximum after only 4 hours; thereafter it

stays more or less constant as long as the tracer input is not stopped. After its cessation (t> 24 hours) the concentration at the source point falls rapidly; needless to mention that below 20 m (i.e., below the thermocline) virtually no tracer mass can be discerned. At the position 720 m towards west (b), the concentration in the epilimnion grows first to a maximum, then rapidly decreases after the cessation of the wind to a new minimum to reach a second maximum that is attained 30 hours later. This second maximum is due to the backward swing to the west of the surface water, a fact that is corroborated by the plots of the horizontal velocity components shown in Fig.13. At the other off-central positions (Fig.12 c, d, e, f) the time at which the maximum concentration is reached is shifted to later times depending on how large the distance of the considered position is from the position of the source. A second maximum is not or not clearly attained. The value of the maximum concentration at the position towards west (b), is far smaller than those of positions south and east of it. Consider next a tracer source at a position in the middle of the Obersee. Time series of the concentration at the position of the source (a) and west (b), east (c) and south (d) of it are shown in Fig. 14 a - d as are the components of the horizontal velocity (e), (f). The concentration-time series also exhibit small oscillations but these have smaller periods (11 hours) and are clearly related to the Poincaré waves seen in Fig. 14 e, f. The Kelvin wave is also seen in the longitudinal velocity components, but this period (of ~100 hours) can only be seen in the tracer-concentration-time series at the position west of the source (Fig. 14 b).

Generally, the tracer concentration initially grows, reaches a maximum and decreases rapidly after wind cessation. This is not so for the point upstream of the source (panel b) where this maximum is attained after 80 hours only. This delay is obviously the effect of advection and the two relative maxima seen in Fig. 14 b are the coupling with the small though present Kelvin-type velocity oscillations in the long direction seen in Fig. 14 e.

Fig. 15 shows the time series of the tracer concentration 3 km off-shore from a point between Romanshorn and Arbon. Conditions how the tracer is brought in are being described in the figure caption. The behaviour is similar to that observed in Fig. 14; appreciable values for the concentration are restricted to the upper 20 metres, the influence of the advection due to the Kelvin wave, which is much stronger in this near-shore position than in the position of Fig. 14, see Fig.~16, is very strong in the position 1.2 km downstream of the source position (Fig. 14 b). The concentration one day after the wind cessation i.e., two days after the cut-off of the tracer inflow is about four times as large as the first maximum is when the tracer inflow is stopped. This must be due to the backswing of the longitudinal surface velocities in the Kelvin wave (Fig. 16). Some traces of Poincaré-type waves can also be seen, but except for Fig. 15 d they are very small.

While the above results seem to indicate that because of the strong stratification tracer mass cannot reach the hypolimnion in appreciable values this is not so at locations where strong downwelling occurs. Fig.17 demonstrates this for a position very close to the western end of Überlinger See. Interesting are in particular the panels (c) and (d) which show the concentration-time series at two positions 1.2 km and 2.0 km east of the central source position. At times 75 - 120 hours after commencement of the experiment the concentrations at the 30 - 50 m depths are considerably

higher than they are in the upper layer at those times.

mployed by us with the mesh of 65×17 grid points. Notice that the boundary from which the coordinate net was constructed by conformal mapping does not everywhere coincide with the shoreline. The island Mainau and the segment Rorschach-Bregenz are spared out, and the shorelines are indicated by thick lines in these regions.

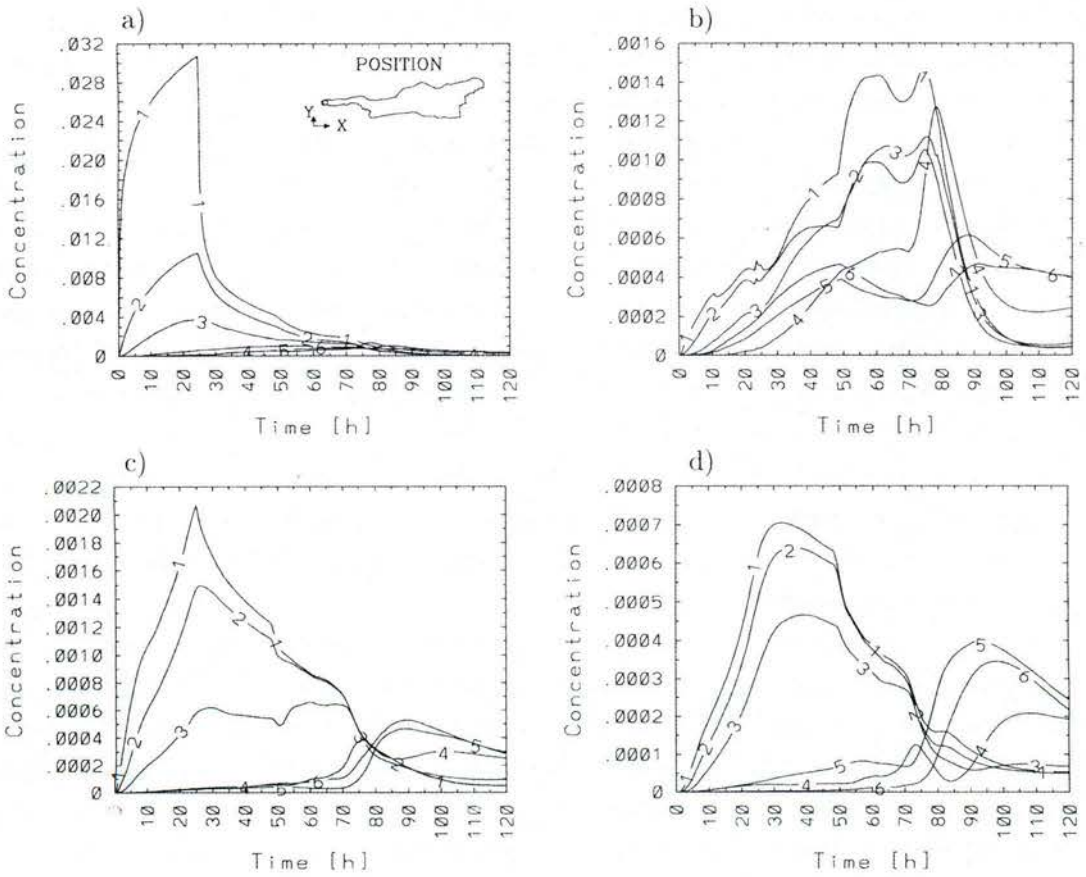

Fig. 17 Stratified Lake Constance

Time series of the tracer concentration at the western end of Überlinger See, for a tracer input centered at a position 1.4 km off-shore over a surface area of 1 000× 100 m^2 and an intensity of 20 $mg \cdot m^{-2} \cdot s^{-1}$. Panel (a) is at the center of the tracer input, (b) is 800 m towards west, (c) is 1.2 km towards east and (d) is 2 km towards east. The tracer and wind scenarios are otherwise the same as in previous figures.

7. Concluding remarks

In this paper we studied tracer dispersion in lakes by using a semi-implicit semi-spectral numerical model based on SPEM (Haidvogel *et al*, 1991, Wang & Hutter, 1999). By employing the σ-transformation in the vertical and using a curvilinear coordinate system in the horizontal the lake domain is transformed into a unit cube, employing a spectral expansion of the unknown

functions in the vertical direction in terms of Chebyshev polynomials and using finite differences in the horizontal directions. To achieve as far as possible a stable numerical integration scheme an implicit integration routine was used in the vertical direction making the new code considerably more stable than the original SPEM was. The used upwind finite differencing in the advective terms of the diffusion equation was particularly important to achieve (i) numerical stability and (ii) to restrict the computed values for the concentration to positive real values. The hydrodynamic equations are coupled with the diffusion equation via these advective terms. We employed it a priori estimates for the turbulent viscosities, constant in time, but adjusted to the initial mass distribution (homogeneous versus stratified lake).

As the early time response to impulsively applied winds is crucial in tracer dispersion problems at these times the high concentrations in the near-source region are rapidly and effectively reduced it was important to demonstrate that the wave mechanisms that are important in lakes are also seen in the evolving tracer concentrations, at least at early times. In homogeneous water inertial oscillations are accompanied with the main flow, in stratified waters these are the Kelvin- and Poincaré-type waves. That traces of these wave patterns could be made out in the tracer concentrations in an ideal rectangular basin of constant depth as well as in Lake Constance is a partial check of the suitability of the discretized model.

For a tracer source on the free surface it was found that in homogeneous water the tracer was relatively rapidly dispersed over the entire water depth, whilst in stratified water the same tracer mass is by and large dispersed in the epilimnion with some, though limited, transport into the hypolimnion where large downwelling occurs.

A number of problems remained unresolved and need be attacked in further analyses. One of these problems is the use of upwind differencing schemes in the advective terms. By employing these the transport properties of the advective terms could properly be accounted for; however it is known that these schemes are accompanied with a relatively large amount of numerical diffusion. Higher order upwind differencing techniques are a possible avenue to improve the code in this regard. Another problem is to employ substructuring techniques where the computations turn out to be too rough with the use of the present scheme. These topics will be dealt with in upcoming papers.

Acknowledgements

We acknowlege financial support from the Deutsche Forschungsgemeinschaft and the A. v. Humboldt Foundation and the Max Planck Society through K. Hutter's Max Planck Prize. We thank Ms. Danner for her help with typing the text.

References

Haidvogel, D.,B.,Wilkin, J.,L., and Young, R. 1991. A Semi-Spectral Primitive Equation Ocean-Circulation Model Using Vertical Sigma and Orthogonal Curvilinear HorizontalCoordinates. *Journal of Computational Physics.* 94: 151-185.

Hutter, K. 1984. Fundamental Equations and Approximations. Hydrodynamics of Lakes, CISM-Lectures Hutter, K. (Ed.), Springer-Verlag, Vienna-New York.

Hutter, K. 1986. Hydrodynamic Modelling of Lakes. Transport Phenomena in the Environment, Gulf Publishing Company, Houston. pp. 897-998.

Maiss, M., Ilmberger, J., Zenger, A., and Münnich, K.O. 1994a. A SF_6 tracer study of horizontal mixing in Lake Constance. *Aquatic Sciences*, 56/4, Birkh äuser Verlag, Basel.

Maiss, M., Ilmberger, J., and Münnich, K.O. 1994b. Vertical mixing in Überlingersee (Lake Constance) traced by A SF_6 and heat. *Aquatic Sciences*, 56/4, Birkhäuser Verlag, Basel.

Peeters, F. 1994. Horizontale Mischung in Seen. Dissertation, ETH Zürich.

Wang, Y .1996. Windgetriebene Strömungen in einem Rechteckbecken und im Bodensee. ShakerVerlag, Aachen. Dissertation, Institute of Mechanics, Technical University Darmstadt.

Wang, Y., and Hutter, K.1996. A semi-implicit semi-spectral primitive equation model for lake circulation dynamics and its stability performance, *J. of Computational Physics,* 139: 209-241.